UNDERSTANDING THE PROCESSABILITY OF GRAPHITE BLEND ELECTRODES WITH SILICON NANOPARTICLES

Diana Zapata Dominguez[1], Alejandro A. Franco[1, 2, 3, 4]**

[1]Laboratoire de Réactivite et Chimie des Solides (LRCS), UMR CNRS 7314, Université de Picardie Jules Verne, Hub de l'Energie, 15, rue Baudelocque, 80039 Amiens Cedex, France.

[2]Réseau sur le Stockage Electrochimique de l'Energie (RS2E), FR CNRS 3459, Hub de L'Energie, 15, rue Baudelocque, 80039 Amiens Cedex, France

[3]ALISTORE-European Research Institute, FR CNRS 3104, Hub de l'Energie, 15, rue Baudelocque, 80039 Amiens Cedex, France.

[4]Institut Universitaire de France, 103 Boulevard Saint Michel, 75005 Paris, France

**Corresponding contact author: alejandro.franco@u-picardie.fr

Abstract

The manufacturing process aims to optimize the parameters leading to enhanced Lithium-Ion Battery (LiB) electrode properties. Particularly, developing silicon/graphite blends could be an alternative for boosting LiB energy density while using the longstanding properties of graphite. Here, we report the manufacturing parameters impact of the mixing, coating, and calendering steps on the properties of silicon/graphite blend electrodes. The mixing process was assessed by the solid and silicon content dependency, where the viscosity increases when increasing the solid and decreasing the silicon content. Moreover, the slurry rheology directly impacts the mechanical stability of the electrode when coating using thicker comma gaps. The calendering step evidences a porosity threshold necessary for adequate ionic resistance and cycling life. We found that porosities between 45% to 56% for these silicon/graphite blends yield higher performance. Lower than 30% porosity highly impacts the electrochemical performance in a detrimental way.

Keywords Li-ion batteries, silicon nanoparticles, graphite, anodes, calendering, slurry

1. Introduction

Lithium-ion batteries (LiBs) have increased over the last three decades, being today the best choice for energy storage due to their cyclability, larger capacity, and high power. Numerous challenges need to be tackled given the increasing use of electric vehicle applications, such as achieving higher energy density and power densities.[1–3] Active materials that accommodate further Li-ions could improve the LiB energy density. Silicon is a promising active material due to its almost ten times higher theoretical capacity (3576 mAh/g) than commercial graphite (372 mAh/g). Nevertheless, silicon undergoes a significant volume change upon cycling that provokes electric connectivity loss from the current collector and increased strain, reducing cycle life. Improving silicon cycling issues has become crucial for advanced electric vehicles LiBs.[4,5] Several strategies can improve silicon cycling problematics, such as carbon-coated nanostructured electrodes, which have demonstrated a better-cycled life and improved pulverization by avoiding direct contact with the electrolyte and forming a well-behaved solid electrolyte interphase (SEI).[6–9] Furthermore, mixing silicon with graphite to develop composites has improved aging behavior and capacity retention by creating a conductive matrix that sustains silicon volume expansion.[10–12]

A growing interest in improving LiBs cycle life is also linked to optimizing the battery manufacturing process. This process includes multiple steps, such as the slurry preparation and the coating, solvent drying, electrode calendering, and cell assembly. Optimizing the fabrication steps aims to improve the energy density, cycling rate, and stability. Since silicon has recently been added to advanced batteries, few studies have addressed the optimization of the manufacturing steps. Today, much of the silicon added in advanced batteries for electric vehicles is combined with graphite. In particular, Si is added in low contents (< 10% wt) to boost the electrode capacity while buffering silicon volume expansion and benefiting from the well-behaved graphite cycling.

The slurry optimization research has led to the coupling effect of slurry formulation with the electrochemical performance. For instance, electrode slurries that utilize PAA as binder lead to good dispersion but the poorest cycling compared with LiPAA. The slurry rheology shows a ten times higher capacity for LiPAA than PAA binder-based slurries.[13] Comparably, Karkar *et al.* demonstrated that using CMC in Si-carbon nanoplatelets blends led to higher viscosity than PAA. They attributed this to higher CMC molecular mass (700 K *vs.* 450 K for PAA) because of the more rigid CMC polymeric backbone and poorer charge density that unbalanced the attractive interparticle force.[14] The Si size influence has been studied in the slurry rheology with 35% solid content, revealing a higher viscosity for Si nanoparticle-graphite blends (Si Nps/Gr) than Si microparticle-graphite blends (Si μps/Gr).[15] Another helpful technique is to perform frequency sweeps, where the storage (G') and loss (G") modulus can provide hints about the slurry stability and microstructure. However, these slurry studies are reported less frequently.[16] Returning to Si size dependence, frequency sweep results displayed an elastic response for Si Nps/Gr (G'> G") contrary to Si μps/Gr (G"> G'), which offered a viscous-like behavior. These imply that while Si (Nps/Gr will result in a homogeneous mass loading coating, Si Nps/Gr will lead to a stable slurry, avoiding particle settling after prolonged rest.[15]

Regarding calendering and porosity optimization, Jeschull *et al.* have focused on the graphite particle size impact on the capacity retention and coulombic efficiency of graphite-silicon blends, leading to improved electrochemical efficiency when using smaller graphite particles.[11] Karkar *et al.* demonstrated that calendering decreases the cycle stability in Si/Carbon nanoplatelets/CMC electrodes due to the break of particle-binder bridges, decreasing the electrode' mechanical strength.[17] Other calendering studies suggest that porous structures collapse under high pressure.[18]

Herein, we report the effect of mixing, coating, and calendering manufacturing parameters in the slurry rheology, morphology, microstructured, and

electrochemical performance of silicon nanoparticles and graphite blends (Si/Gr). Our study presents the correlation of the solid and silicon content on the slurry rheology, the comma gap effect on the electrode microstructured, and the calendering percentage on the ionic resistance and the electrochemical performance. Considering that manufacturing optimization is needed to calibrate the machine learning and physical models, these results can be used to validate manufacturing process simulations as the ones carried out in our ARTISTIC project and adjust industrial electrode fabrication.[19–22]

2. Results and discussion

Different Si/Gr blend anodes were prepared for rheological, morphology, and electrochemical investigation. Rheology measurements were conducted to evaluate the impact of solid content and electrode formulation on the viscosity *vs*. applied shear rate profile and further rheological properties of the slurry. Details on sample preparation and experimental conditions are presented in Methods. Afterward, we discuss the effect of the comma gap and calendering on the coating electrode microstructured and electrochemical cycled behavior using two different Si/Gr blend slurries.

2.1 Rheology characterization of slurry anode formulations

SOLID CONTENT DEPENDENCY IN THE SLURRY RHEOLOGY

Figure 1 shows slurries containing a similar electrode formulation with 8% Si/83% Gr and different solid content percentages (24, 26, and 27). The solid content presented here were chosen allowed us to well-dispersed the selected formulation. Higher solid contents lead us to mushy-like slurries and lost fluidity. The viscosity changes when varying the solid content (Figure 1a). The viscosity of the suspension is decreased over the entire shear rate when decreasing the solid content (SC), from 27 to SC 24. This difference can be explained considering that additional particle agregation may occur at higher solid contents because of particle jamming and clustering. Thus, a

supplementary shear force is necessary when friction appears.[23] The decrease in viscosity is higher at lower shear rate rates when using lower solid contents (varying from 64 to 24 Pa s, for SC 37 to 24, respectively). In contrast, this decrease is lessened at higher shear rates, following other studies that compared the solid content in cathode slurries. Nevertheless, the coating of these slurries would be nearly identical; slurry casting with SC 24 should be more uniform because of its lower viscosity.[24]

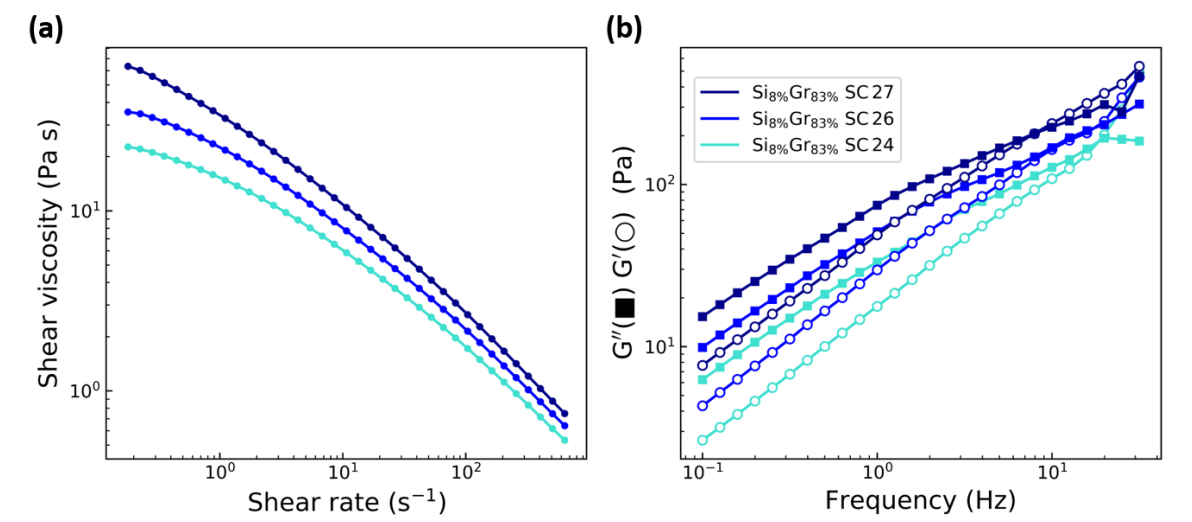

Figure 1. (a) Rotational viscosity and **(b)** oscillatory frequency sweep measurements of slurries with different solid contents containing 8% Si/ 83% Gr blends with 2% CB45, and 7% Na-CMC. Markers ■ and ○ refers to G" (viscous modulus) and G' (elastic modulus), respectively.

Figure 1b shows the frequency sweep by maintaining the strain constant as the applied frequency is increased. The frequency sweeps give information on the storage (G') and loss (G") modulus, also known as elastic and viscous modulus, respectively. For the three solid contents used in the slurry formulation, the obtained G" is larger than G' at the whole frequency interval until ~ 10^1 Hz, showing a predominantly viscous behavior. At this frequency, the tendency is reversed (G'> G"), indicating an elastic behavior. Indeed, when decreasing solid content, the frequency value, at which the tendency is inverted, is shifted to

higher frequencies, given 8, 10, and 20 Hz for solid contents of 27, 26, and 24, respectively.

Si CONTENT DEPENDENCY AND PARTICLE SHAPE IN THE SLURRY RHEOLOGY

After evaluating the solid content effect on the rheological properties of the 8% Si/83% Gr formulation, we assessed the viscosity dependency on the Si content. We also prepared a pure graphite formulation containing 91% Gr to compare the viscosity. The solid content was kept constant at SC 26.

The shear viscosity *vs.* shear rate is presented in Figure 2a. The viscosity decreases when increasing the Si content from 8% to 15%. Similarly to the solid content dependency on the viscosity, at lower shear rates, the differences in viscosity are more significant, increasing doubly from 9, 17, to 34 Pa s for 15%, 11%, and 8% Si, respectively, contrary to at higher shear rates (0.46, 0.54, and 0.63 Pa s for 15%, 11%, and 8% Si, respectively). Compared with pure graphite, the slurry viscosity is at least ten times more than the viscosity in 8% Si/83% Gr formulation for the same solid content. It was necessary to add water (reaching a solid content of 21) to have a viscosity comparable with the 8% and 11% Si formulations at higher shear rates. This difference can be explained by considering that an irregular particle surface or shape such as the one in graphite presents higher viscosity because of more contact points, thus additional inter-particle friction.[25] SEM images evidence the irregular shape of the graphite particles, with sizes ranging from 5 to 20 μm (see Figure 3a). Si Nps particles are mainly rounded and organized between the graphite grains, with sizes ranging from 5 to 90 nm (see Figure 3b), indicating the higher viscosity of pure Gr when using SC 26.

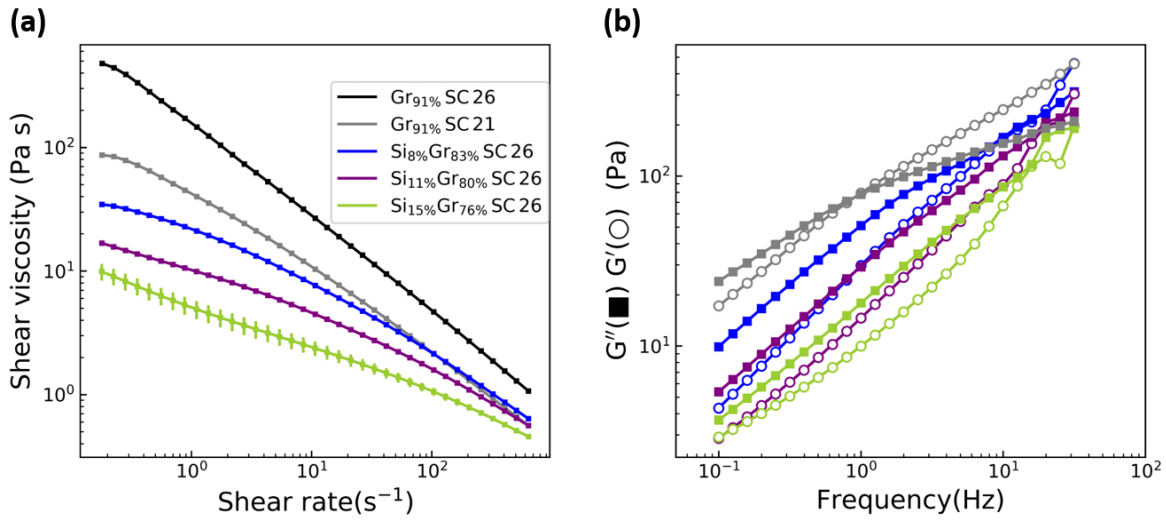

Figure 2. (a) Rotational viscosity and **(b)** oscillatory frequency sweep measurements of slurries with different Si and Gr contents (0% Si/100%Gr, 8% Si/83% Gr, 11%Si/80% Gr, and 15%Si/76%Gr) with 2% CB45, and 7% Na-CMC and a solid content of 26. Markers ■ and ○ refers to G" (viscous modulus) and G' (elastic modulus), respectively.

Figure 2b shows the frequency sweeps for the slurries with different Si content and pure graphite with a solid content of 21. For the pure graphite, G" is higher at a lower frequency, indicating a viscous-like behavior. After 0.88 Hz, this tendency changes to G'> G" with an elastic response. Comparing the slurries with Si content, we observe that the slurry formulation with higher Gr content (8% Si / 83% Gr) presents a tendency closer to pure Gr than the 15% Si/ 76% Gr; only G'> G" happens at a higher frequency. Few studies have reported the rheology changes with Si content variation in the slurry formulation. Andersson *et al.* reported opposite results, showing an elastic and viscous response when having pure Si and pure Gr, respectively.[15] Nevertheless, the solid content was changed by them when necessary, indicating that particle-particle interactions may change considerably when solid fractions are not controlled, reducing the friction and, thus, affecting the viscous and elastic modulus response.

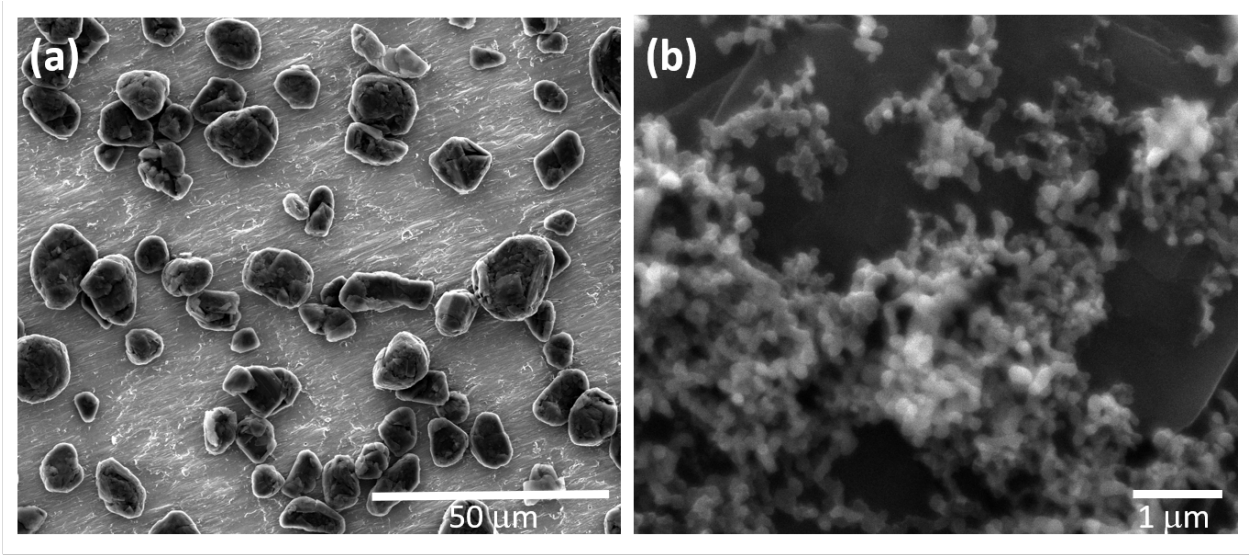

Figure 3. SEM images of **(a)** Graphite particles and **(b)** Si Nps.

2.2 Slurry coating and electrode calendering

Additionally, the coating and calendering parameters are evaluated to ensure high-quality electrodes and adequate electrochemical performance. The slurries contained 8%Si/83%Gr, and 15%Si/76%Gr bends were cast to analyze the macrostructural information when changing the manufacturing parameters. For instance, we evaluate the practical limit for the comma gap when coating and the effect of pressure on the tortuosity when calendaring that affect the output properties of the electrodes.

COMMA GAP EFFECT ON THE ELECTRODE MACROSTRUCTURE

The relationship between the coating comma gap, electrode thickness, mass loading, and porosity are now assessed for the 8%Si/83%Gr slurry blend. Details on the coating parameters are presented in Methods. Table 1 shows the resulting electrode properties when coating using 0.3 m/min line speed. When coating the 8%Si/83%Gr slurry blend, the comma gap and the resulting electrode's mass loading vary linearly. The porosity is nearly independent of the mass loading and the used casting gap.

Table 1. Main characteristics of the dried electrodes when using a comma gap of 100, 200, and 300 μm: compositions, porosity, thickness, and mass loading.

Comma gap [μm]	100	200	300
Calculated shear rate [Hz]	50	25	16
Porosity [%]	62 ± 2	59 ± 3	57 ± 2
Thickness [μm]	54 ± 1	82±2	100.8 ± 0.8
Mass loading [mg/cm^2]	2.9 ± 0.2	5.3±0.4	7.3 ± 0.1

Surface and cross-sectional SEM images show the morphology of the electrodes when using a comma gap of 100 and 300 μm. The surface SEM images show that the big graphite grains are well distributed over the electrode and surrounded by lighter grey particles (see Figure 4a and c, respectively).

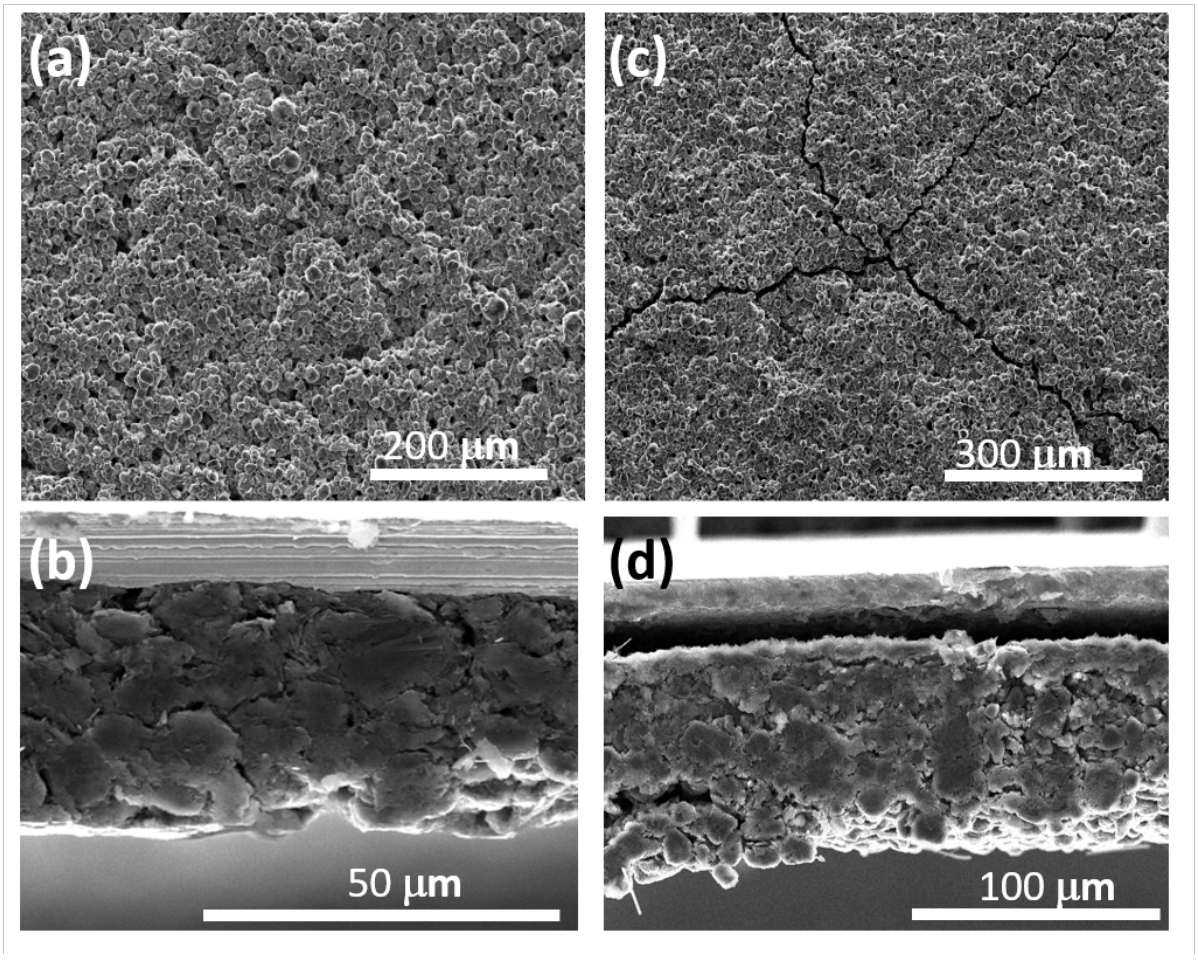

Figure 4. Surface and cross-sectional SEM images of the 8%Si/83%Gr blend coated using a comma gap of 100 μm **(a)** and **(b)**, 300 μm **(c)** and **(d)**, respectively.

The cross-sectional images evidence the contact of the electrode with the current collector. For the comma gap of 100 μm, the electrode has solid contact with the copper collector, contrary to the electrode coated a 300 μm, where there is a cavity between the current collector and the casted electrode (see Figure 4b and d, respectively), causing cracking over the electrode (see Figure 4c). This lack of contact between the electrode and the current collector could be due to a poorer slurry contact with the copper foil, thus higher surface tension.[16] The surface energy can be enhanced by oxidizing or texturizing the copper to improve the interaction between the slurry and the correct collector. In this case, the oxide groups in the current collector could bind more effectively with the CMC binder, and the rough-surface Cu foil could have a higher surface area and tighter contact between Si and Gr.[26] Otherwise, the slurry's surface tension can be reduced by adding a cosolvent such as isopropanol.[16]

An alternative explanation for the cracks formed in this thick electrode could be the mixing sequence that may affect the casted properties of the electrode. In our slurry methodology, we mixed the active materials and conductive additive with the CMC binder, which may have facilitated a gel-like formation (see Figure 1b, G' > G" at 10 Hz). This gel-like may render a higher surface tension slurry that could not be suitable for thicker electrode preparation. In contrast, it does not affect when coating thinner electrodes down to 54 ± 1 μm.[16]

CALENDERING AND TORTUOSITY EFFECT ON THE ELECTRODE MACROSTRUCTURE AND ELECTROCHEMICAL PERFORMANCE

After accessing the comma gap's influence on the mesostructured electrode, we characterize the electrodes using two different Si contents when coated using a comma gap of 200 μm. The comma gap chosen is suited for prototype electrochemical applications, and the electrode thickness allows us to investigate the calendaring effect on the electrochemical performance. The electrodes were calendered at 10%, 20%, and 30% of their initial thickness. Additional information on the calendered procedure is presented in Methods.

Table 2 shows the resulted electrode properties. As expected, the porosity decreases when decreasing the calendered gap with initial porosities of 59 ± 3% and 56 ± 1%, for 8%Si/83%Gr and 15%Si/76%Gr, respectively, following precedent studies where the Si/Gr blends present a porosity between 50-70%.[10,11,17] We will evaluate the impact of these porosities on the electrode properties since it is known that the volume changes when silicon-based materials are cycled. Consequently, finding an adequate compromise between the porosity is necessary, while volume expansion can be accommodated and ensure a satisfactory Si cycling process.

Table 2. Main characteristics of the dried electrodes when using a comma gap of 200 μm and two different formulations: calendered gap, mass loading, thickness, and porosity.

Electrode		Calender gap [μm]	Mass loading [mg/cm^2]	Thickness [μm]	Porosity [%]
8%Si/83%Gr	Pristine	0	5.3 ± 0.4	82 ± 2	59 ± 3
8%Si/83%Gr	Calendered 10%	74 ± 5		71 ± 1	50.7 ± 0.8
8%Si/83%Gr	Calendered 20%	52 ± 6		65 ± 1	44.7 ± 0.9
8%Si/83%Gr	Calendered 30%	37 ± 4		55 ± 1	30 ± 2
15%Si/76%Gr	Pristine	0	5.8 ± 0.1	80 ± 2	56 ± 1
15%Si/76%Gr	Calendered 10%	70 ± 6		71 ± 1	47 ± 1
15%Si/76%Gr	Calendered 20%	60 ± 5		62.2 ± 0.5	37.2 ± 0.6
15%Si/76%Gr	Calendered 30%	32 ± 3		57.8 ± 0.3	29.8 ± 0.5

Figure 5 shows cross-sectional SEM images of the electrodes depending on the Si content in the formulation and the calendered percentage. The pristine electrodes are shown in Figure 5a and e for Si8% and Si15%, respectively. The graphite grains are preferentially oriented along with the coating plane, and the silicon particles (lighter in gray) agglomerate between the graphite grains, as observed by other studies.[17,27]

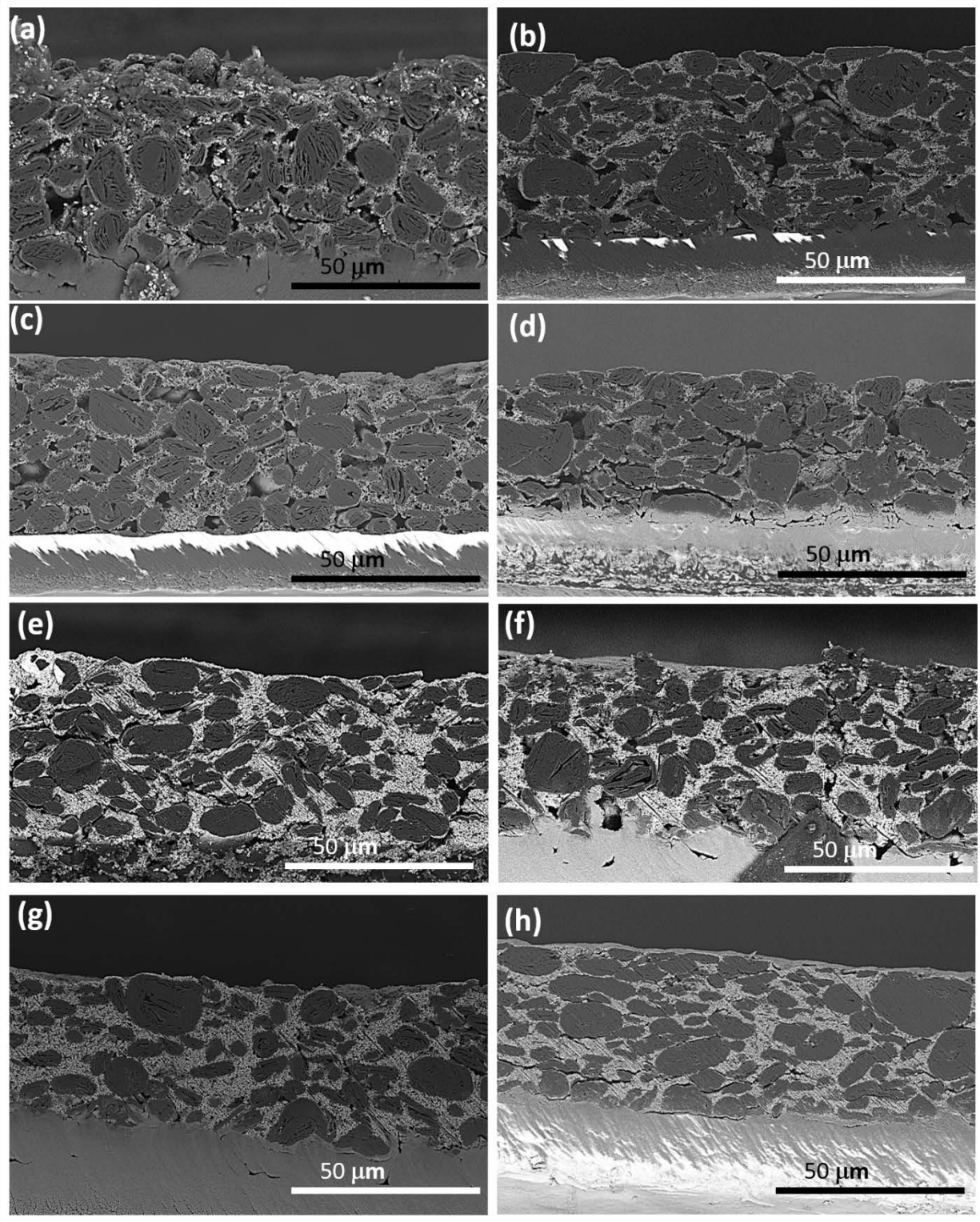

Figure 5. Cross-sectional SEM images for the formulation Si8%/Gr83% **(a)** pristine, calendered **(b)** 10%, **(c)** 20%, **(d)** 30% of the thickness and for the formulation Si15%/Gr76% **(e)** pristine, calendered **(f)** 10%, **(g)** 20%, **(h)** 30% of the thickness.

The formulation with Si 8% appears to have an increased porosity due to the lower content of Si, leaving more free space among the Gr grains than the formulation with Si 15%. In other words, the electrode surface in the Si15%/Gr76% formulation seems to be better exploited, filled by the Si Nps.

As the calendar percentage increased, the apparent porosity observed in the pristine electrodes decreased, as observed in Table 2. It can also be noted that the calendering process orients the graphite grains (preferentially with a flat shape) adjacent to the current collector. The graphite grains seem to cluster at the electrode surface and bottom, as expected when using a roll-press.[27,28] The two compositions of Si differentiate in the porous shape and size when calendering. For instance, the appearance of the pores in the Si 8% is mainly rounded, arranged vertically, and larger. In contrast, the pores present in the Si15% are oriented horizontally with a scratch-like shape and are smaller.

Calendering improves the energy density and optimizes the electron transport through the electrode bulk. When the electrode thickness is decreased, the contact between the electrode components is improved. Nevertheless, the ion transport decreases, and the electrode tortuosity factor increases.[16]

Symmetric cell studies provide more information on the internal pore resistance without interference from a counter electrode (lithium metal) and charge-transfer reactions (lithium intercalation). This approach reflects the ionic resistance (R_{ion}) in the pores of the electrode bulk.[29–31] To get more insight into the porous ionic resistance in the electrodes, we performed symmetric cell impedance studies using negative electrodes with the Si8%/Gr83% and Si15%/Gr76% formulation depending on the calendered percentage (see Figure 6a and b, respectively).

The experimental Nyquist plots for both formulations present mainly a typical electrical blocking behavior with a slope of 45° from the real axis and constant real impedance in the high-frequency and low-frequency regions, respectively (see Figure 6a and b). The Nyquist plots for the Si15% electrodes coincide between the pristine, calendered 10% electrodes. The R_{ion} is slightly higher for

the 20% electrode (see Figure 6b). In contrast, the R_{ion} value for the electrode calendered at 30% is the highest, as observed for the Si8%/Gr83% formulation with 29% – 30% porosities.

Interestingly, the Si8% formulation calendered 20% presents the lowest R_{ion} (porosity of 44.7 ± 0.9%, see Table 2). The Nyquist plots for the pristine and 10% calendered electrode mostly overlap (see Figure 6a), giving a similar R_{ion}.

Contrary to positive electrodes such as NMC and LFP, the ionic resistance in pores progressively decreases when calendering.[29,32,33] Here, we observed the lowest ionic resistance corresponding to a specific or range of calendered percentages for the Si8% and Si15% contents, respectively. The ion resistances are the maximum for the electrode calendered at 30% for both formulations. In comparison, the calendar percentage does not change the ion resistance significantly for the Si15% formulation. The lowest ion resistance is achieved when calendering 20% of the Si8%/Gr83% electrode.

Looking at low-frequency regions in Figure 6a and b, we observe differences in the inclination of the Nyquist plot for the different samples. Contrary to perfect non-faradaic processes, the transition of the Rion region to lower frequencies should be a constant real impedance. This inclination tendency could be due to a small charge-transfer resistance of the anions ClO_4^- present in the electrolyte (10 mM $TBAClO_4$ in 1:1 wt% EC:DMC). Nevertheless, EC solvates the anion slugging the intercalation.[34] Abbas *et al.* reported that anions ClO_4^- could intercalate the graphite sheets (capacity = 20 mAh/g) when using a highly concentrated aqueous electrolyte because of Gr defects and lower crystallinity.[35]

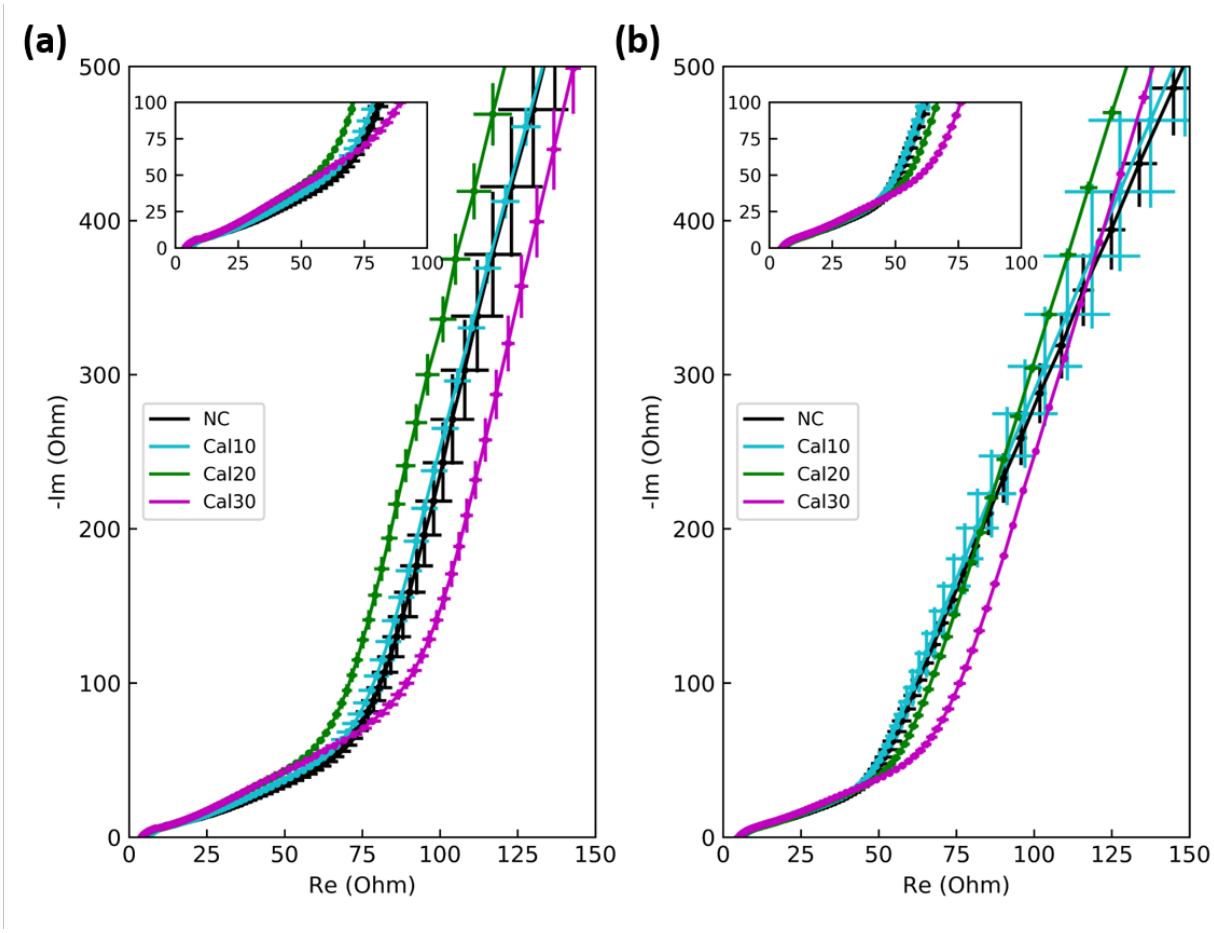

Figure 6. Nyquist plots for symmetric cells using two negative electrodes for the **(a)** Si8%/Gr83% and **(b)** Si15%/Gr76% formulations at the pristine, calendered: 10%, 20%, and 30% of the thickness in 10 mM $TBAClO_4$ in 1:1 wt% EC:DMC at 25 °C.

Calendering impacts the cycling performance in the electrode. Consequently, we evaluated the electrochemical cycling (normalized charge capacity *vs.* cycle number) for the Si8%/Gr83% and Si15%/Gr76% formulations (see Figure 7a and b, respectively) for the pristine and calendered electrodes. More details on the electrochemical cycling procedure can be found in Methods.

The calendered percentage highly influences the electrochemical performance. The Si8% electrode calendered at 20% has the highest charge capacity over cycles, followed by the pristine and the calendered 10%. In comparison, the Si15% electrode charge capacity is enhanced for the pristine and calendered

10%. The worst cycling performance for both formulations corresponds to the electrode calendered 30%.

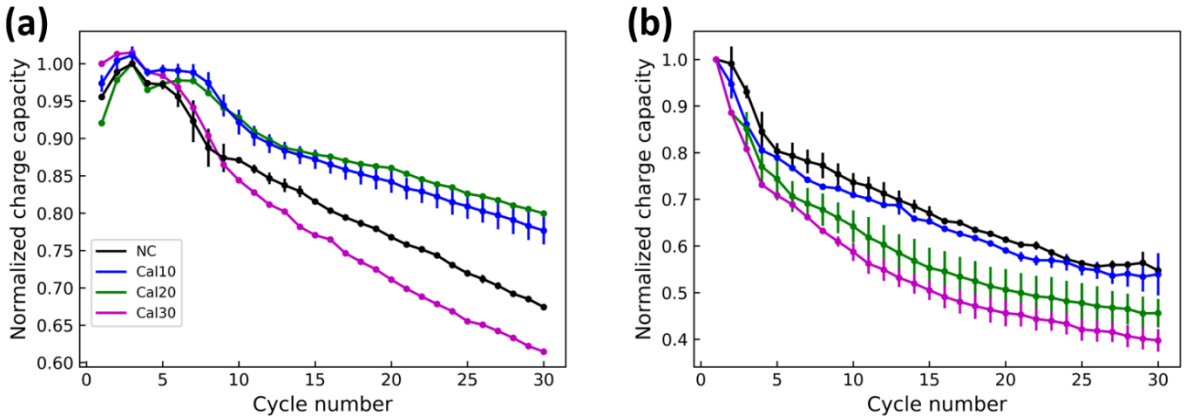

Figure 7. Normalized charge capacity for **(a)** Si8%/Gr83% and **(b)** Si15%/Gr76% of the pristine, calendered 10%, 20%, and 30% of the thickness.

Remarkably, the cycling performance results are consistent with the impedance studies shown in Figure 6a and b. Accordingly, the charge capacity improves as the ion resistance decreases. For instance, the electrode with 8% Si calendered at 20% of the thickness presents the lowest ion resistance, evidencing the improved cycling capacity (see Figure 6a). In comparison, the electrodes calendered at 30% show the highest ion resistances for both Si8% and Si15% formulations(see Figure 6a and b). Both impedance behaviors are directly linked with cycling performance. As shown in Table 2, the electrodes' porosity decreases when the calendered percentage increases. An optimized porosity will lead to appropriate void spaces for silicon volume expansion while assuring a gain in the volumetric capacity and good mechanical properties. Previous works in Si/carbon black blend electrodes reported that an increased calendered pressure leads to poor electrochemical performance due to the break of particles and particle-binder bonds.[17,36] In comparison, adding graphite to silicon electrodes while calendering the electrodes seems to improve capacity retention. The authors explained that graphite is a lubricous material that may allow the

particles to glide against each other instead of fracturing after pressing the electrode.[37]

An overall decrease in cycling performance is observed with increased Si content. For instance, after 30 cycles, the Si15% electrodes have a charge capacity between 30% and 60%. In comparison, the Si8% formulation electrodes present 60%–80% charge capacity, improved when calendered to 45% porosity. It appears that the graphite content for the Si15% electrode is insufficient to improve the electrochemical performance considerably. Therefore, a porosity between 46% to 57% may probably lead to acceptable but insufficient cycling performance. This result could indicate that other parameters need to be considered to improve the cycle life when using higher contents of silicon, such as engineering the matrix electrode structure to contain the silicon cycling problematics when incrementing its content.

3. Conclusion

In this paper, we analyzed the manufacturing processability of Si Nps/graphite blend electrodes, considering the effects of mixing, coating, and calendering on the electrode morphology and electrochemical performance. More particularly, we evaluated the solid and silicon content dependency on the slurry rheology. As expected, the viscosity increases when the solid content increases, showing a viscous and elastic-like behavior at low and high frequencies, respectively. Regarding the Si content impact on the slurry, the formulation with lower Si content is more viscous due to a more significant presence of graphite with an irregular particle shape, increasing the interparticle friction. The slurry rheology impact on the coating was studied through different comma gaps. The electrodes coated at 300 μm detached from the current collector, while the electrodes coated at lower comma gap showed appropriate adhesion properties. Then, symmetric cell measurements and cycling performance allowed us to evaluate the calendering effect on the coated electrodes for Si8% and Si15% formulations. The

highest electrochemical performances are reached for the electrodes with the lowest ionic resistance. The Si8%/Gr83% electrode corresponds to a porosity of 45% (calendered 20% of the thickness). In comparison, the Si15%/Gr76% electrode showed acceptable but insufficient cycling performance for porosities between 46% and 57%, indicating that a higher level of engineering is needed to improve the performance. Finally, we believe that manufacturing process data and parameter correlations are useful for calibration and validation of physical and machine learning models, as we have evidence in the ARTISTIC project.

4. Methods

In order to prepare the electrode, we used silicon nanoparticles (Si Nps). We employed C-NERGYTM super C45 carbon black (CB) supplied by IMERYS. Na-CMC was used as a binder and purchased from Sigma-Aldrich. The slurry components (8%, 11%, 15% Si Nps, 83%, 80%, and 76% graphite, 2 % CB, and 7 % Na-CMC) were premixed with a soft blender. Afterward, water was added until reaching a desired solid content (SC) of 27%, 26%, or 24%, a ratio between the solid components and the solvent. The mixture was performed in a Dispermat CV3-PLUS high-shear mixer for 2 hours 30 min a water-bath cooled recipient at 25 ºC. The slurry was coated over a 16 μm copper current collector using a comma-coater prototype-grade machine (PDL250, People & Technology, Korea), fixing the gap at 100, 200, and 300 μm and the coating speed at 0.3 m/min. The electrodes were dried in a built-in two-part oven at 60 and 65 ºC. The electrodes were calendered with a prototype-grade lap press calender (BPN250, People & Technology, Korea). The latter consists of a two-roll compactor of 25 cm in diameter. The gap between the rolls was set to reach 10%, 20%, and 30 % of compression. The calendering was performed at constant line speed (0.54 m/min) and 60 ºC.

Porosities were calculated according to

$$\varepsilon = 1 - \frac{m_{el}\,(X_{Si}/\rho_{Si} + X_{Gr}/\rho_{Gr} + X_{CB}/\rho_{CB} + X_{Na-CMC}/\rho_{Na-CMC})}{V_{el}} \qquad \text{Eq. 1}$$

where X and ρ are the mass fractions in the electrode and densities of the three solid components Si/Gr/CB/Na-CMC and m_{el} and V_{el} correspond to the electrode mass and volume, respectively.

The SEM images were acquired with a SEM-FEG Zeiss crossbeam Neon40 using a voltage of 5 kV. The electrodes were polished through ionic cryo-polishing under a high vacuum to obtain a smoother surface. Leica EM TIC 3X Ion Beam Slope was used with three broad convergent beams of Ar^+ on a static tungsten carbide mask.

The properties of the electrodes are presented in Table 1and Table 2. EIS tests for calculating the tortuosity were performed in 2035 coin cells assembled in a dry room (H_2O < 15 ppm). The coin cells (both on the positive and negative side) were assembled using Celgard 2500 as separator (thickness = 25 µm, porosity = 55%, mass = 2.25 mg), Si/Gr blends (diameter = 13 mm), positive and negative casing (mass = 0.8715 and 0.8606 g, respectively), two current collectors (thickness = 0.5 and 1.0 mm, mass = 0.758 and 1.541 g, respectively), and a spring (mass = 0.1780 g). The electrolyte was a 10 mM $TBAClO_4$ solution, prepared in a 1:1 wt mixture of ethylene carbonate:dimethyl carbonate (volume = 100 µL, mass = 0.148 g). The EIS tests were performed with an MTZ-35 impedance analyzer (BioLogic, Seyssinet-Pariset, France) in 10^{-1} – 10^7 Hz with a potential perturbation of 5 mV. All measurements were carried out at 25 ± 1°C.

Electrochemical characterization was performed in 2032 coin cells in a half-cell configuration with a Li counter/reference electrode. A 1 M $LiPF_6$ solution in ethylene carbonate: dimethyl carbonate (1:1 wt.%) + 10% FEC was used as the electrolyte. The half-cells were assembled in a glovebox (Braun) with a H_2O and

O_2 content lower than 0.1 ppm. The galvanostatic charge/discharge experiments were carried out using a BCS-810 series battery cycler (BioLogic, Seyssinet-Pariset, France) in the voltage range of 1.5 – 0.01 V. The half-cells were cycled three times at C/10, with a floating current at the end of lithiation corresponding to C/50. The following cycles were performed C/5 with a floating current at C/20 at the end of lithiation.

Acknowledgements

A.A.F. and D.Z.D. acknowledge the European Union's Horizon 2020 research and innovation program for the funding support through the European Research Council (grant agreement 772873, "ARTISTIC" project). A.A.F. acknowledges Institut Universitaire de France for the support. We thankfully acknowledge Imène Esteve and Stéphanie Delbrel from the Institut de Minéralogie, de Physique des Matériaux et de Cosmochimie (IMPMC, UMR 7590) facilities, in which the ionic polishing/SEM experiments were performed, supported by Région Île-de-France (grant SESAME 2006 NOI-07-593/R, INSU-CNRS, INP-CNRS, UPMC) and the French National Research Agency (ANR) (grant ANR-07-BLAN-0124-01).

Bibliography

1. Chu, S. & Majumdar, A. Opportunities and challenges for a sustainable energy future. *Nature* **488,** 294–303 (2012).

2. Goodenough, J. B. & Park, K.-S. The Li-Ion Rechargeable Battery: A Perspective. *J. Am. Chem. Soc.* **135,** 1167–1176 (2013).

3. Duan, J. *et al.* Building Safe Lithium-Ion Batteries for Electric Vehicles: A Review. *Electrochem. Energy Rev.* **3,** 1–42 (2020).

4. McDowell, M. T., Lee, S. W., Nix, W. D. & Cui, Y. 25th Anniversary Article: Understanding the Lithiation of Silicon and Other Alloying Anodes for

Lithium-Ion Batteries. *Adv. Mater.* **25,** 4966–4985 (2013).

5. Obrovac, M. N. & Chevrier, V. L. Alloy Negative Electrodes for Li-Ion Batteries. *Chem. Rev.* **114,** 11444–11502 (2014).

6. Hassan, F. M., Chabot, V., Elsayed, A. R., Xiao, X. & Chen, Z. Engineered Si Electrode Nanoarchitecture: A Scalable Postfabrication Treatment for the Production of Next-Generation Li-Ion Batteries. *Nano Lett.* **14,** 277–283 (2014).

7. Bernard, P., Alper, J. P., Haon, C., Herlin-Boime, N. & Chandesris, M. Electrochemical Analysis of Silicon Nanoparticle Lithiation – Effect of Crystallinity and Carbon Coating Quantity. *J. Power Sources* **435,** 226769(1–9) (2019).

8. Sourice, J. *et al.* One-Step Synthesis of Si@C Nanoparticles by Laser Pyrolysis: High-Capacity Anode Material for Lithium-Ion Batteries. *ACS Appl. Mater. Interfaces* **7,** 6637–6644 (2015).

9. Sourice, J. *et al.* Core-Shell Amorphous Silicon-Carbon Nanoparticles for High-Performance Anodes in Lithium-Ion Batteries. *J. Power Sources* **328,** 527–535 (2016).

10. Wetjen, M. *et al.* Differentiating the Degradation Phenomena in Silicon-Graphite Electrodes for Lithium-Ion Batteries. *J. Electrochem. Soc.* **164,** A2840–A2852 (2017).

11. Jeschull, F. *et al.* Graphite Particle-Size Induced Morphological and Performance Changes of Graphite–Silicon Electrodes. *J. Electrochem. Soc.* **167,** 100535 (2020).

12. Jeschull, F. *et al.* Electrochemistry and Morphology of Graphite Negative Electrodes Containing Silicon as Capacity-Enhancing Electrode Additive. *Electrochim. Acta* **320,** 134602 (2019).

13. Armstrong, B. L. *et al.* Role of silicon-graphite homogeneity as promoted by

low molecular weight dispersants. *J. Power Sources* **517,** 230671 (2022).

14. Karkar, Z., Guyomard, D., Roué, L. & Lestriez, B. A Comparative Study of Polyacrylic acid (PAA) and Carboxymethyl Cellulose (CMC) Binders for Si-based Electrodes. *Electrochim. Acta* **258,** 453–466 (2017).

15. Andersson, R., Hernández, G., Edström, K. & Mindemark, J. Micro versus Nano: Impact of Particle Size on the Flow Characteristics of Silicon Anode Slurries. *Energy Technol.* **8,** 2000056 (2020).

16. Li, J., Fleetwood, J., Hawley, W. B. & Kays, W. From Materials to Cell: State-of-the-Art and Prospective Technologies for Lithium-Ion Battery Electrode Processing. *Chem. Rev.* **122,** 903–956 (2022).

17. Karkar, Z. *et al.* How Silicon Electrodes Can Be Calendered without Altering their Mechanical Strength and Cycle Life. *J. Power Sources* **371,** 136–147 (2017).

18. Son, Y. *et al.* Calendering-Compatible Macroporous Architecture for Silicon–Graphite Composite toward High-Energy Lithium-Ion Batteries. *Adv. Mater.* **32,** 2003286 (2020).

19. ARTISTIC web page. Available at: http://www.erc-artistic.eu/. (Accessed: 10th June 2022)

20. Liu, C., Arcelus, O., Lombardo, T., Oularbi, H. & Franco, A. A. Towards a 3D-resolved model of Si/Graphite composite electrodes from manufacturing simulations. *J. Power Sources* **512,** 230486 (2021).

21. Ngandjong, A. C. *et al.* Investigating electrode calendering and its impact on electrochemical performance by means of a new discrete element method model: Towards a digital twin of Li-Ion battery manufacturing. *J. Power Sources* **485,** 229320 (2021).

22. Lombardo, T. *et al.* The ARTISTIC Online Calculator: Exploring the Impact of Lithium-Ion Battery Electrode Manufacturing Parameters Interactively

Through Your Browser. *Batter. Supercaps* **5,** (2022).

23. Stickel, J. J. & Powell, R. L. Fluid Mechanics and Rheology of Dense Suspensions. *Annu. Rev. Fluid Mech.* **37,** 129–149 (2005).

24. Ouyang, L. *et al.* The effect of Solid Content on the Rheological Properties and Microstructures of a Li-ion Battery Cathode Slurry. *RSC Adv.* **10,** 19360–19370 (2020).

25. Brenner, H. Rheology of a Dilute Suspension of Axisymmetric Brownian Particles. *Int. J. Multiph. Flow* **1,** 195–341 (1974).

26. Yang, Y. *et al.* A review on Structuralized Current Collectors for High-Performance Lithium-Ion Battery Anodes. *Appl. Energy* **276,** 115464 (2020).

27. Etiemble, A. *et al.* Evolution of the 3D Microstructure of a Si-Based Electrode for Li-Ion Batteries Investigated by FIB/SEM Tomography. *J. Electrochem. Soc.* **163,** A1550–A1559 (2016).

28. Etiemble, A. *et al.* Multiscale morphological characterization of process induced heterogeneities in blended positive electrodes for lithium–ion batteries. *J. Mater. Sci.* **52,** 3576–3596 (2017).

29. Landesfeind, J., Hattendorff, J., Ehrl, A., Wall, W. A. & Gasteiger, H. A. Tortuosity Determination of Battery Electrodes and Separators by Impedance Spectroscopy. *J. Electrochem. Soc.* **163,** A1373–A1387 (2016).

30. Ogihara, N. *et al.* Theoretical and Experimental Analysis of Porous Electrodes for Lithium-Ion Batteries by Electrochemical Impedance Spectroscopy Using a Symmetric Cell. *J. Electrochem. Soc.* **159,** A1034–A1039 (2012).

31. Ogihara, N. & Itou, Y. Impedance Analysis Using Symmetric Cells for Understanding Electrochemical Behaviour of Porous Electrodes for Lithium-ion Batteries. *R&D Rev. Toyota CRDL* **48,** 17–24 (2017).

32. van Bommel, A. & Divigalpitiya, R. Effect of Calendering LiFePO 4 Electrodes. *J. Electrochem. Soc.* **159,** A1791–A1795 (2012).

33. Ogihara, N., Itou, Y., Sasaki, T. & Takeuchi, Y. Impedance Spectroscopy Characterization of Porous Electrodes under Different Electrode Thickness Using a Symmetric Cell for High-Performance Lithium-Ion Batteries. *J. Phys. Chem. C* **119,** 4612–4619 (2015).

34. Gao, J., Tian, S., Qi, L. & Wang, H. Intercalation manners of perchlorate anion into graphite electrode from organic solutions. *Electrochim. Acta* **176,** 22–27 (2015).

35. Abbas, G. *et al.* Influence of structural properties on (de-)intercalation of ClO4− anion in graphite from concentrated aqueous electrolyte. *Carbon N. Y.* **186,** 612–623 (2022).

36. Nguyen, B. P. N., Chazelle, S., Cerbelaud, M., Porcher, W. & Lestriez, B. Manufacturing of industry-relevant silicon negative composite electrodes for lithium ion-cells. *J. Power Sources* **262,** 112–122 (2014).

37. Du, Z., Dunlap, R. A. & Obrovac, M. N. High Energy Density Calendered Si Alloy/Graphite Anodes. *J. Electrochem. Soc.* **161,** A1698–A1705 (2014).